Sb-doped zirconium dioxide submicron fibers for separation of pertechnetate (TcO4-) from aqueous solutions

Lönnrot, Satu

2020-10-07

Lönnrot , S , Paajanen , J , Suorsa , V , Zhang , W , Ritala , M & Koivula , R 2020 , '
Sb-doped zirconium dioxide submicron fibers for separation of pertechnetate (TcO4-) from
aqueous solutions ' , Separation science and technology , vol. 56 , no. 14 , pp. 2338-2350 . https://doi.org/10.1080/0

http://hdl.handle.net/10138/333271
https://doi.org/10.1080/01496395.2020.1826967

Taylor & Francis
Taylor & Francis Group

SEPARATION SCIENCE AND TECHNOLOGY

Separation Science and Technology

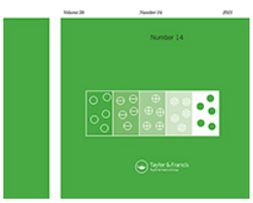

ISSN: (Print) (Online) Journal homepage: https://www.tandfonline.com/loi/lsst20

Sb-doped zirconium dioxide submicron fibers for separation of pertechnetate (TcO_4^-) from aqueous solutions

Satu Lönnrot, Johanna Paajanen, Valtteri Suorsa, Wenzhong Zhang, Mikko Ritala & Risto Koivula

To cite this article: Satu Lönnrot, Johanna Paajanen, Valtteri Suorsa, Wenzhong Zhang, Mikko Ritala & Risto Koivula (2021) Sb-doped zirconium dioxide submicron fibers for separation of pertechnetate (TcO_4^-) from aqueous solutions, Separation Science and Technology, 56:14, 2338-2350, DOI: 10.1080/01496395.2020.1826967

To link to this article: https://doi.org/10.1080/01496395.2020.1826967

SEPARATION SCIENCE AND TECHNOLOGY
2021, VOL. 56, NO. 14, 2338–2350
https://doi.org/10.1080/01496395.2020.1826967

Taylor & Francis
Taylor & Francis Group

Sb-doped zirconium dioxide submicron fibers for separation of pertechnetate (TcO_4^-) from aqueous solutions

Satu Lönnrot, Johanna Paajanen, Valtteri Suorsa, Wenzhong Zhang, Mikko Ritala, and Risto Koivula

Department of Chemistry, University of Helsinki, Helsinki, Finland

ABSTRACT

Submicron ZrO_2 fibers with three different Sb-doping levels (5, 10 and 15 cation%) were produced with an electroblowing synthesis for removal of $^{99}TcO_4^-$. The Sb-doped ZrO_2 fibers showed high selectivity toward $^{99}TcO_4^-$, which was not interfered by ClO_4^-, NO_3^- or Cl^- ions and showed no selectivity toward ReO_4^-. The optimal pH range for the ^{99}Tc separation was 2–6 but the Sb-doped fibers maintained very high uptake level throughout the studied pH range of 1–10. According to the uptake experiments, Sb(III) is assumed to reduce Tc(VII) to Tc(IV) that is then adsorbed by the zirconia surface.

ARTICLE HISTORY
Received 16 May 2020
Accepted 15 September 2020

KEYWORDS
Technetium; ZrO_2; electroblowing; reduction; antimony doping

Introduction

Technetium-99 (^{99}Tc) is a fission product of ^{235}U fission that is generated in nuclear reactors with a high cumulative yield of 6.13%.[1] Tc is the lightest element without stable isotopes but it has long-lived isotopes including beta emitting ^{99}Tc with a half-life of 211 100 years.[1] Due to the long half-life and high mobility of pertechnetate anion (TcO_4^-), efficient decontamination methods are necessary to avoid severe radiological contamination of the environment. Tc has multiple oxidation states (-I – VII) but the predominant species is the heptavalent TcO_4^- that is thermodynamically stable in oxidized aqueous solutions. The second most stable oxidation state is Tc(IV) that is prevailing in a moderately reducing environment.[2,3] Tc(IV) has multiple oxo/hydroxyl species TcO^{2+}, $TcO(OH)^+$, $TcO(OH)_2$ and $TcO(OH)_3^-$ of which $TcO(OH)_2$ prevails in the pH range from 2.5 to 10.9, the positively charged TcO^{2+} and $Tc(OH)^+$ species below pH 2.5, and the negatively charged $TcO(OH)_3^-$ above pH 10.9.[3] The other oxidation states of Tc such as V and VI can form in specific conditions but they disproportionate readily back to Tc(IV) and Tc(VII).[2] Instead, oxidation states III and lower can be obtained in highly reducing environment but they are oxidized easily.[2] For research, Tc is only available as radioactive tracers that is preventing its use in experimental facilities without license for radioactive work. Therefore, many researchers have used rhenium as a comparable surrogate for Tc because also Re prevails as heptavalent ReO_4^- and can undergo redox reactions. However, the slight differences between TcO_4^- and ReO_4^- can have a significant impact on separation.

The removal of TcO_4^- is commonly based on ion exchange, adsorption or reductive separation.[4,5] However, performances of ion exchange resins and adsorbents often suffer from the presence of other ions, and organic resins are prone to radiation damage.[6] For that reason, several inorganic materials have been developed for more selective removal of TcO_4^- and ReO_4^- such as mesoporous alumina,[7] metal-organic frameworks,[8,9,10,11] zero valent iron (ZVI),[12,13] Fe_2O_3 and Fe_3O_4[12] and zirconium dioxide nanoparticles anchored onto reduced graphene oxide (ZrO_2@rGO).[14] In addition, universal nonselective sorbent materials including activated carbon have been utilized in TcO_4^- removal.[15,16,17] Li *et al.*[18] observed that after TcO_4^- was remediated by porous iron, Tc(VII) was mainly reduced to Tc(IV) and co-precipitated with FeO(OH) and Fe_3O_4 or incorporated into their structure. Even though the ZVI materials show good potential for TcO_4^- uptake, these materials have their limitations such as low surface area and susceptibility for leaching.[18,19,20] In addition to ZVI, also other materials have shown potential for reductive separation. Koivula *et al.*[21] observed that Sb-doped SnO_2 was able to efficiently separate TcO_4^- from water solutions. The Tc uptake was suggested to be a combination of reduction and anion exchange as the sorption behavior could not be explained only with one mechanism. Because of a rather low reduction potential of Sb(III), it should

CONTACT Satu Lönnrot satu.lonnrot@helsinki.fi Department of Chemistry, University of Helsinki, Helsinki, Finland
Supplemental data for this article can be accessed on the publisher's website.

favor Tc(VII) reduction over Re(VII) due to the higher oxidation potential of Tc(VII). However, the low point of zero charge (pH_{PZC}) of SnO_2 retards the anion separation above pH_{PZC} due to the electrostatic repulsion that leaves room for further material improvement.

Electroblowing is a simple method for production of organic and inorganic nano- and submicron fibers.[22,23,24] The method is a combination of electrospinning and blow spinning techniques having the best properties of these two methods. A voltage difference between a spinneret needle and a collector is producing single untangled fibers whereas gas blowing is improving the fiber production rate by multiple orders.[25] A precursor solution used for the fiber synthesis can be diverse. When only solvents and polymer are used, the resulting product is fully organic, but addition of inorganic precursor to the synthesis solution enables manufacturing of inorganic fibers when the polymer support is combusted after the spinning process. The process has been applied, for example, in a synthesis of ZrO_2 fibers.[26,27] ZrO_2 is an inorganic material with excellent properties for an adsorbent as it is nontoxic, chemically and physically inert and practically insoluble to water. Various crystal structures,[28,29,30] morphologies,-[31,32,33,34] and amphoteric nature of ZrO_2[35] make the material an excellent choice for adsorbent design. Therefore, several papers have been published about its uptake properties for a great number of elements with different oxidation states, particularly for oxy-anions. For example, Su *et al.*[36] reported phosphate removal by mesoporous ZrO_2 nanosorbent and Cui *et al.*[37] studied As(III) and As(V) separation with amorphous zirconium oxide nanoparticles. Moreover, ZrO_2 submicron fibers have been used for Sb(V) separation.[26,27] Lönnrot *et al.*-[26] presented that ZrO_2 submicron fibers built up less pressure in a packed bed column than small particles but the fibers still offered large surface area that is necessary for an efficient sorbent.

In this study, we designed and synthesized reductive Sb-doped ZrO_2 submicron fibers for TcO_4^- separation. The electroblowing synthesis was developed to produce fibers whose frame composed of tetragonal ZrO_2 which is an active structure in heavy metal separation, and Sb(III) was incorporated into the ZrO_2 lattice to selectively reduce TcO_4^- from aqueous solutions. Altogether, three Sb-doping levels, 5, 10 and 15 cation%, and undoped ZrO_2 were produced to investigate the effect of Sb-doping level on the TcO_4^- uptake. The produced fibers were characterized with several methods and the TcO_4^- uptake properties of Sb-doped ZrO_2 fibers were comprehensively studied. The effect of pH, competing ions and their concentration, and contact time on the Tc uptake was investigated. In addition, the TcO_4^- uptake performance of the Sb-doped fibers was studied with a dynamic column experiment. The role of Sb and Zr in the uptake process was investigated by using Sb and Zr containing commercial materials as comparison samples. Furthermore, we demonstrated differences in the uptake of TcO_4^- and ReO_4^- on the 10%Sb:ZrO_2 fiber.

Materials and methods

Materials

$^{99}TcO_4^-$ was purchased from Eckert and Ziegler and $^{188}ReO_4^-$ was eluted from an $^{188}W/^{188}Re$ generator just before the experiments. All chemicals used in the uptake experiments were analytical grade and used without further purification and solutions were made into deionized water (18.2 MΩ cm at 25°C, MilliQ Millipore). Synthesis chemicals are given in the synthesis section.

Synthesis

ZrO_2 fibers were synthesized by electroblowing a solution containing metal precursors and polyvinylpyrrolidone (PVP, Alfa Aesar, M_w 1 300 000 g mol^{-1}) followed by calcination. For the Sb-doped ZrO_2 fiber synthesis, 15 g of $ZrOCl_2{\cdot}8\ H_2O$ (Merck Supelco, ≥99%) was dissolved in 42 mL of deionized water and $SbCl_3$ (Sigma-Aldrich, ≥99%) was added into 24 mL of ethanol (VWR Chemicals, 99.90%) to achieve the desired doping levels of 5, 10 or 15 cation%. The water solution was then mixed with 84 mL of 14 wt% PVP/ethanol solution and then with the $SbCl_3$ ethanol solution under magnetic stirring until the solution became homogeneous. The precursor solution for the undoped ZrO_2 followed the recipe of Lönnrot *et al.*[26] In a typical spinning process, 10 mL of solution was withdrawn into a syringe and a 0.21 mm ø needle was attached to the syringe tip. The syringe was placed on a syringe pump that was feeding the solution at a rate of 15 mL h^{-1}. The needle was pushed through an adapter of a self-made apparatus, based on the work of Holopainen and Ritala,[22] that feeds air at a flow rate of 40 NL min^{-1}. A high voltage source was used to apply 15 kV potential between the needle and a grounded steel grid collector that composes of a planar back collector at 75 cm distance and a cylindrical side collector. The collector was sealed into a polycarbonate box where the relative humidity was adjusted to 15% at 22°C by leading pressurized air into the box. The electroblown fibrous mats were folded on a shallow porcelain evaporating dish and calcined in air at 350°C for 6 hours using a heating rate of 15°C min^{-1}.

Characterization

Synthesized fibers were coated with 4 nm of Au/Pd alloy and analyzed with a Hitachi S4800 field emission scanning electron microscope (FESEM). Elemental composition of the fibers, ground in the form of powder, was analyzed with a wavelength-dispersive X-ray fluorescence spectrometer (XRF, PANalytical Axios mAX). The redox state of Sb in the fibers was investigated with a self-assembled X-ray absorption spectroscopy (XAS) instrument. The instrument is built in a similar manner as the one designed and described by Honkanen *et al.*[38] The samples were measured through a helium balloon to reduce X-ray attenuation by ambient air between the X-ray source (Mini-focused X-ray tube with Pd target, Micro X-ray), sample and a silicon drifted detector (Amptek XR-100SDD). A Si(400) crystal analyzer (ESRF) was used to select the energy range for the measurement. A powder X-ray diffractogram (XRD) was measured from the powdered fibers using a PANalytical X'Pert^3 Powder diffractometer with Cu K_α radiation. A thermogravimetric analysis coupled with a simultaneous differential thermal analysis (TGA-STDA, Mettler Toledo TA8000) was conducted for uncalcined fibers from 25°C to 800°C using a heating rate of 10°C min^{-1} in a flow of air. Fibers before and after calcination were analyzed with Fourier-transform infrared attenuated total reflectance (FTIR-ATR, Bruker Alpha Platinum ATR) from 360 to 4000 cm^{-1} with a 2 cm^{-1} resolution. N_2 adsorption–desorption isotherms were obtained at 77 K on a Micromeritics ASAP 2010 automated analyzer. Specific surface areas were estimated according to the Brunauer-Emmett-Teller (BET) method, and the pore size distributions were calculated using the Barrett–Joyner–Halenda (BJH) method based on the adsorption branch. The samples were preconditioned in vacuum at 300°C.

Zeta potentials of the fibers were determined from pH 1 to 10. In the experiment, 10 mg of fibers was mixed with 10 mL of 0.01 M NaCl solution and equilibrated for 24 h before the equilibrium pH measurement and zeta potential determination with a Zetasizer Nano ZC. After the zeta potential analysis, the antimony concentration in the solution of the 10%Sb:ZrO_2 fiber samples was measured using an Agilent 4200 Microwave Plasma – Atomic Emission Spectroscopy (MP-AES) in a hydride generation mode and the zirconium concentration with a normal mode.

Uptake experiments

Effect of pH on Tc uptake. The effect of pH on the TcO_4^- adsorption was examined from pH 1 to 10 in normal atmospheric conditions. Samples composed of 10 mg of fibers and 10 mL of 20 kBq L^{-1} $^{99}TcO_4^-$ ($2.21{\cdot}10^{-7}$ M) in 0.01 M NaCl solution the pH of which was set into a range of 1 to 10 with a small volume of either HCl or NaOH. After 24 hours of constant rotary mixing, the equilibrium pHs were determined and samples phase separated by 2100 *g* centrifugation and 0.2 µm syringe filtration. The separation efficiency was determined by mixing 2 mL of the filtrate with 8 mL of Optiphase HiSafe 3 scintillation cocktail and measuring the remaining activity with a Perkin Elmer Tri-Carb 2910TR liquid scintillation counter. A comparative pH effect experiment was done for $^{188}ReO_4^-$ with the 10%Sb:ZrO_2 fibers that had the best uptake properties for TcO_4^-. The experiment was conducted otherwise similarly as the technetium experiments but 250 kBq L^{-1} ($2.54{\cdot}10^{-14}$ M) $^{188}ReO_4^-$ was added instead of $^{99}TcO_4^-$ and the filtered 8 mL samples were analyzed with a PerkinElmer Wallac Wizard 3" 1480 automatic gamma counter.

Reference samples

The TcO_4^- uptake of fibers was compared with commercial materials m-ZrO_2 (Alfa Aesar, Puratronic 99.978%), Sb_2O_3 (Sigma-Aldrich, trace metal basis 99.99%) and Sb_2O_5 (Aldrich, trace metal basis 99.995%). For all samples, 10 mg of material was weighed into 20 mL vials and 10 mL of solution with 20 kBq L^{-1} $^{99}TcO_4^-$ and 0.01 M NaCl, pH 4.0 was added. Samples were shaken for 24 h before phase separation and activity measurement.

Competing ions

The effect of competing Cl^-, NO_3^-, ClO_4^-, H_3BO_3, SO_4^{2-} and PO_4^{3-} on the TcO_4^- uptake was investigated at pH 4.0 with increasing concentration of competing ion, 0.001–0.2 M. The same TcO_4^- and adsorbent concentrations, and separation method were used as in the pH experiment.

Kinetics

Adsorption kinetics was determined by mixing 80 mg of fibers with 80 mL of solution containing 20 kBq L^{-1} $^{99}TcO_4^-$ in 0.01 M NaCl at pH 4.0 under magnetic stirring. The sample aliquots were withdrawn and filtered at preset time points.

Column separation

The performance of the Sb-doped ZrO_2 fibers was tested in a column operation. A ø 1 cm column was packed with 0.25 g of fibers and 10 kBq L^{-1} $^{99}TcO_4^-$ ($1.11{\cdot}10^{-7}$ M) in 0.01 M NaCl solution with pH 4.0 was fed through the column at a flow rate of 33 mL h^{-1}. The breakthrough of ^{99}Tc from the column was determined by

collecting fractions and measuring their activity by liquid scintillation counting. A similar column with 10%Sb:ZrO_2 was done for 54.2 kBq L^{-1} ($5.51 \cdot 10^{-15}$ M) $^{188}ReO_4^-$ in 0.01 M NaCl solution but the fractions were measured with the gamma counter.

Results calculation

Distribution coefficient (K_d) that describes the distribution of the adsorbate between the adsorbent and solution is presented as follows:

$$K_d = \frac{(C_0 - C_{eq})V}{C_{eq}m} \quad (1)$$

where C_0(Bq L^{-1} or M) is the initial concentration, C_{eq} (Bq L^{-1} or M) is the equilibrium concentration, V(mL) is the volume of the solution and m(g) is mass of a dry adsorbent. When activity concentration is used in the calculation, background is subtracted before applying the activity concentration into the equation. Uncertainty of K_d is calculated using the error propagation law but in a case of extremely high uncertainties (>100%), which are observed when C_{eq} is close to the detection limit, the uncertainty in figures (Fig. 7–9) is estimated to be 90% of the K_d value. The detection limit (DL) and minimum detectable activity (MDA) calculations are presented in a supplementary material, Section A1. Even if the activities were below DL, they are used for the result calculation and DL is presented as a dashed line in the figures.

The uptake percentage is calculated using equation

$$R = \frac{(C_0 - C_{eq}) * 100\%}{C_0} \quad (2)$$

where R is the uptake percentage of technetium and C_0 and C_{eq} are the same as above. Uncertainty is calculated with the error propagation law as such.

Results and discussion

SEM

Eletroblown uncalcined 10%Sb:ZrO_2-PVP fibers have rather smooth surfaces with only few small particles on top of them showing successful synthesis, Fig. 1a. Also, after the calcination that removed the PVP polymer, the fibers have smooth surfaces with no porosity seen with SEM, Fig. 1b-f. On a larger scale, Fig. 1b, it seems that the calcined 10%Sb:ZrO_2 fibers are well separated from each other and have a high length-to-diameter ratio that is typical for electroblown fibers. The high length after the calcination indicates that the fibers are durable and elastic since they tolerate a rather robust handling when the SEM samples are prepared. The mechanical strength is important in separation applications because short pieces of fibers could block separation columns leading to a system failure. When the fibers are inspected more closely, high magnification images show the slightly varying diameter of calcined ZrO_2, 5%Sb:ZrO_2, 10%Sb:ZrO_2 and 15%Sb:ZrO_2 fibers, Fig. 1c,d,e,f. Most of the fibers are round shaped but some have a small portion of flattened or joined fibers due to a slow evaporation of solvents, water and ethanol, during the electroblowing process. Flatness should not negatively affect the uptake capacity of the fibers as the shape is not significantly changing the specific surface area or accessibility of Sb in the structure. Actually, the flatness of the fibers can even increase the specific surface area,

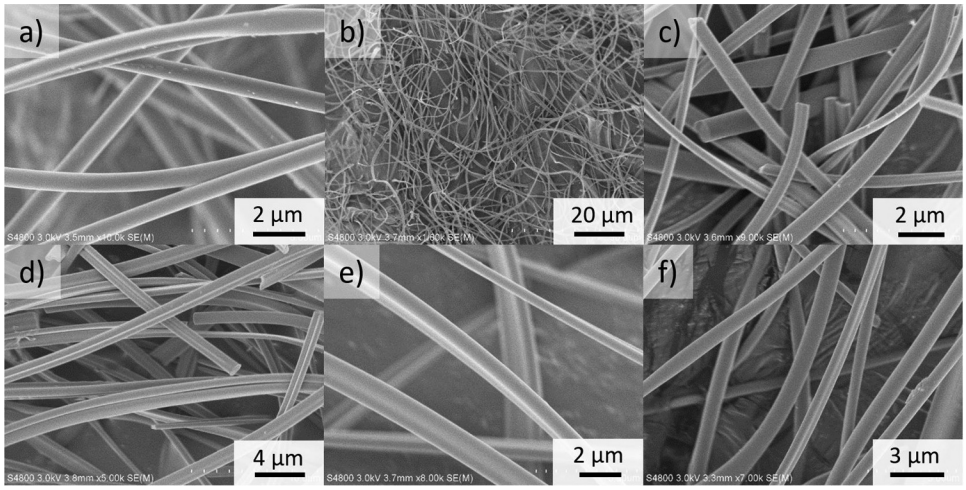

Figure 1. SEM images of a) uncalcined 10%Sb:ZrO_2-PVP fibers b) calcined 10%Sb:ZrO_2 fibers with a low magnification c) ZrO_2 fibers d) 5%Sb:ZrO_2 fibers e) 10%Sb:ZrO_2 fibers and f) 15%Sb:ZrO_2 fibers after calcination with a higher magnification.

important for the ion uptake, as a distorted cylinder shape is creating larger surface with the same mass.

TGA

TG analysis was conducted to inspect the fiber calcination process in a controlled environment even though the analysis of 8 mg samples in TG somewhat differs from the calcination of 0.5 g fiber mats. In the TGA, mass of all fibers decreases in four steps, Fig. 2. In the first step from 25°C to approximately 200°C, remaining solvents, ethanol and water, evaporate that is also observed as an endothermic peak in the STDA. The majority of the mass decreases in the next two steps at 200–380°C and 380–550°C due to the combustion of pyrrolidone side groups of PVP.[39] In the same temperature ranges, two exothermic peaks are observed in the STDA as the combustion of PVP releases heat. The last mass loss step is observed above 600°C, probably due to combustion of the alkane chain of PVP, [39] yielding total mass losses of 72.5%, 68.5%, 68.4% and 68.8% in the order of increasing Sb-doping level. The mass loss of the undoped ZrO_2 is the greatest since the PVP/Zr ratio was the highest in the beginning. The mass of the fibers stabilized above 741°C, 705°C, 688°C and 623°C for respective ZrO_2, 5%Sb:ZrO_2, 10%Sb:ZrO_2 and 15%Sb:ZrO_2, when all organics had combusted. These temperatures seem to follow the order of antimony concentration that could originate from antimony catalyzing the last degradation reaction.

Even though the fibers are calcined at 350°C, the combustion is more efficient than TGA indicates. Upon calcination, the fast heating rate ignites the PVP and the exothermic combustion reaction raises the temperature inside the folded fiber mats higher than the preset temperature. The combustion of the PVP was confirmed with the FTIR analysis of the fibers before and after calcination where the disappearance of the characteristic IR peaks of PVP can be observed, supplementary material Fig. A1 and A2. The FTIR spectra of the calcined fibers show only bending and stretching vibrations of -OH groups originating from coordinated or readsorbed water at 3300, 1575 and 1405 cm^{-1} and Zr-O vibrations at 750 cm^{-1} and below 500 cm^{-1} .[14,40,41] The absence of IR peaks of organic groups confirms the purity of the synthesized products that is essential for the uptake properties of the material as organic residues could cover active surface sites of ZrO_2.

XRD

The calcination process of the fibers was carefully optimized to produce fibers with small tetragonal crystallites that have shown good anion uptake performance in the literature.[26,27] The resulted fibers were analyzed with XRD to confirm that the desired crystallinity was obtained and how the Sb-dopant is behaving in the structure. The XRD diffractograms of all fibers showed dominating tetragonal zirconia (t-ZrO_2) structure, Fig. 3. However, the ZrO_2 and 15%Sb:ZrO_2 fibers also showed a shoulder of monoclinic zirconia (m-ZrO_2) at the 2θ angle of 28.2°. The XRD reflections are relatively broad indicating small crystallite size that is originating from the fast heating rate and the rather low calcination temperature of the fibers. The small crystallite size is beneficial for the ion uptake since it results in larger specific surface area that offers more accessible adsorption sites. In addition, t-ZrO_2 has been calculated to be energetically more suitable for the ReO_4^- adsorption than m-ZrO_2, and that could also be true for TcO_4^-.[14] The doping of

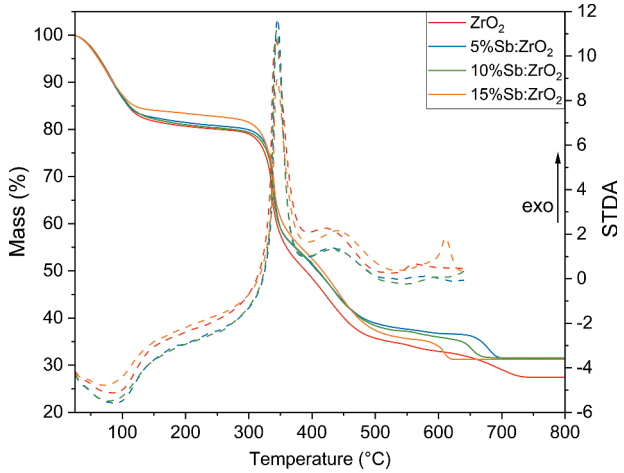

Figure 2. TGA and STDA curves of ZrO_2 and 5, 10 and 15% Sb-doped ZrO_2 fibers.

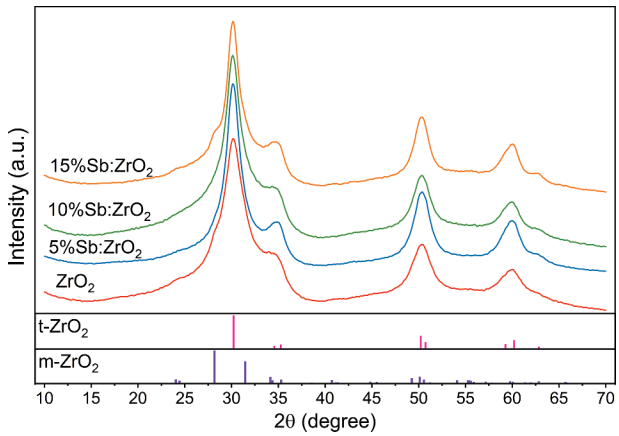

Figure 3. XRD diffractograms of ZrO_2 and three Sb-doped ZrO_2 fibers. The reflections of tetragonal and monoclinic ZrO_2 are presented below the diffractograms.

the fibers did not cause formation of antimony oxide phases that would have resulted in new diffractions. On the other hand, the content of Sb is rather low and the most intensive XRD reflections of Sb_2O_3 and Sb_2O_5 are located in the same 2θ range, 27–35°, as the reflections of ZrO_2 making them nearly impossible to distinguish at such a low concentration and crystallinity. However, as the ionic radii of Sb and Zr are close (6-coordinated Sb(III) 0.76 Å and Sb(V) 0.60 Å and 8-coordinated Zr(IV) 0.84 Å),[42] it is more probable that Sb has replaced Zr in the t-ZrO_2 lattice by forming a solid solution. This kind of replacement has been proposed also for Sb-doped SnO_2 fibers and thin films.[43,44] When a solid solution of metal oxides with different valence forms, charge balance is achieved by a generation of vacancies, substitution pairs or interstitial ions. These crystal defects are generally considered beneficial for the adsorption.[45]

XRF

The Sb/Zr ratio of the Sb-doped fibers was investigated with XRF to semiquantitatively determine the actual Sb-doping level in zirconia since a major loss of Sb could drastically weaken the TcO_4^- uptake properties of the material. The hygroscopic nature of $SbCl_3$, evaporation and segregation of Sb, and material losses during the synthesis could potentially result in unwanted doping levels far from the targeted ratios.[46,47] The XRF analysis (Table A1) showed Sb-doping levels of 3.7, 6.0 and 11.5 cation% of total metal (Sb + Zr) when the theoretical values in the same order were 5, 10 and 15 cation%. However, as the analysis method is only semiquantitative, the concentrations can actually be closer to the target values than the analyzed values indicate. Despite the possible loss of Sb, the remaining amount of Sb in the fibers is more than enough to separate trace amounts of Tc from aqueous solutions. The XRF results also showed some chloride and hafnium residues. The chloride originates from the synthesis chemicals $SbCl_3$ and $ZrOCl_2$ although most of it evaporates during the synthesis. Hafnium in turn originates from $ZrOCl_2$ as the Zr source minerals ZrO_2 and $ZrSiO_4$ accumulate both Zr and Hf due to their chemical similarity, which also makes their separation difficult.[48] Although the fibers contained minute amounts of Cl and Hf, they should not affect the Tc uptake significantly since they are not competing with TcO_4^- or influencing the properties of ZrO_2 noticeably.

XAS

The XAS analysis was conducted to determine the oxidation state of Sb in the fibers, Fig. 4. Sb was added into the synthesis solution as a trivalent $SbCl_3$, but Sb(III) can be oxidized to Sb(V) during the synthesis and particularly in the calcination process. According to the XAS analysis, the calcined 5%Sb:ZrO_2 and 15%Sb:ZrO_2 fibers clearly contained large portions of both Sb(III) and Sb(V) oxidation states since their XANES peaks were spreading over the Sb(III) and Sb(V) energies. The result indicates that partial oxidation of Sb(III) was actually occurring during the synthesis since the calcination process cannot be fully controlled. The rapid heating that was needed to obtain high surface area fibers with a small crystallite size can also be responsible for the oxidation of Sb as an autogenous combustion is a highly oxidative process. In contrast to the 5%Sb:ZrO_2 and 15%Sb:ZrO_2 fibers, the 10%Sb:ZrO_2 fibers contained mainly Sb(III) before the Tc column loading whereas after the Tc column loading Sb(III) was almost fully oxidized to Sb(V) probably due to the oxidation by TcO_4^- and dissolved O_2. However, the oxidation of Sb(III) by O_2 is a slow process,[49] and therefore Sb(III) has time to reduce the heptavalent TcO_4^- to the tetravalent $TcO(OH)_2$. Despite the differences in the initial Sb(III)/Sb(V) ratios, all the Sb-doped fibers contained significant amounts of Sb(III) that is sufficient for the reduction and uptake of trace amounts of technetium. Unfortunately, a rather low signal intensity (laboratory X-ray source), small absorption step of Sb, and measurement at room temperature, which is broadening the XAS edges, prevent quantitative calculations of the Sb oxidation state ratios. The data quality could be significantly improved with a high x-ray flux synchrotron measurement but access to those facilities is limited.

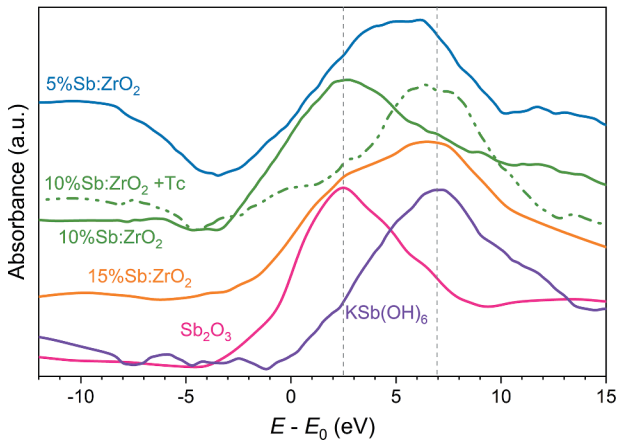

Figure 4. XAS Sb L_I-edge absorption spectra of Sb_2O_3 and $KSb(OH)_6$ chemicals as references for Sb(III) and Sb(V), 5%Sb:ZrO_2, 10%Sb:ZrO_2 and 15%Sb:ZrO_2 fibers, and Tc loaded 10%Sb:ZrO_2 fiber.

BET

The specific surface areas and porosities of the fibers were analyzed with the N_2 adsorption-desorption method, Fig. A3 and A4, and Table 1. The specific surface areas were quite similar for all the fibers with the values ranging from 43 to 59 $m^2\ g^{-1}$. Since the specific surface area of 5%Sb:ZrO_2 is the highest, though with a small margin, it should offer the greatest amount of surface sites for the technetium uptake. Instead, the 10%Sb:ZrO_2 fibers with the lowest specific surface area have the highest uptake capacity in the column experiment seen later. Thus, within the range measured here, the specific surface area might have only a small significance in the Tc remediation. More probably, the amount of Sb(III) in the fibers is limiting the Tc uptake since the oxidation of Sb(III) to Sb(V) was observed in the XAS analysis after the Tc uptake (Fig. 4). The total pore volumes of the fibers are in the range from 0.02 to 0.05 $cm^3\ g^{-1}$ being the lowest for 10%Sb:ZrO_2 and the highest for 15%Sb:ZrO_2. The high pore volume is beneficial for uptake if the pores are sufficiently large for a target ion to enter. The observed pore size distribution was wide but concentrated on micropores with ≤2 nm diameter.

Zeta potential. Zeta potentials of ZrO_2, 5%Sb:ZrO_2, 10%Sb:ZrO_2 and 15%Sb:ZrO_2 were determined from pH 1 to 10, Fig. 5. The maximum zeta potential values were observed at pH 3 and the values decreased gradually toward lower and higher pH values. The approximated pH_{pzc} values in 0.01 M NaCl were 6.3, 6.1, 5.9 and 5.8 in the order of increasing Sb-doping level indicating that Sb lowers the pH_{pzc}. A similar trend was observed when the pH was below pH_{pzc} as the zeta potential values were decreasing in the same order. Consequently, if the separation of TcO_4^- would purely be based on the electrostatic attraction between the TcO_4^- anion and the positively charged fiber surface, the separation should be the highest at pH below pH_{pzc} and decrease when pH is higher than pH_{pzc}. This was actually observed in the pH experiment, Fig. 6. However, the separation cannot be explained only with the electrostatic attraction between TcO_4^- and the fiber surface, which would practically exclude anion uptake above the pH_{PZC} of the materials, and then the ZrO_2 fiber with the highest zeta potential should have offered the best TcO_4^- separation, and neither of these was the case.

Table 1. BET specific surface areas and total pore volumes of the ZrO_2 and three Sb-doped ZrO_2 fibers.

	A_{BET} ($m^2\ g^{-1}$)	V_{pore} ($cm^3\ g^{-1}$)
ZrO_2	49	0.04
5%Sb:ZrO_2	59	0.03
10%Sb:ZrO_2	43	0.02
15%Sb:ZrO_2	54	0.05

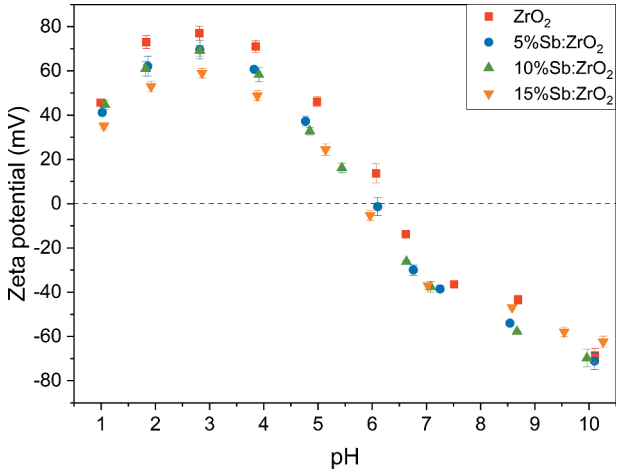

Figure 5. Zeta potential of the fibers as function of pH_{eq} in 0.01 M NaCl with 1 g L^{-1} adsorbent concentration.

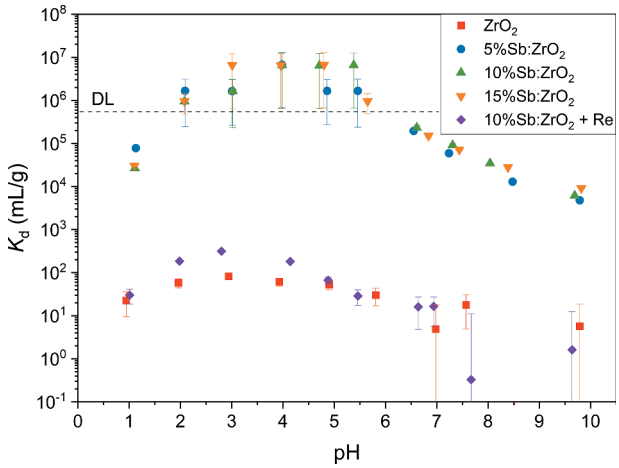

Figure 6. Distribution coefficient (K_d) of 20 kBq L^{-1} TcO_4^- as a function of pH_{eq} in 0.01 M NaCl solution using 1 g L^{-1} adsorbent concentration and K_d of 250 kBq L^{-1} ReO_4^- for 10%Sb:ZrO_2. DL for 99Tc is 0.04 Bq mL^{-1}.

The MP-AES measurement revealed a low solubility of Sb from the 10%Sb:ZrO_2 fibers, Fig. A5. The maximum Sb dissolution, observed at pH 9.9, was below 1.4% of the total amount and the lowest solubility of Sb was 0.2% detected at pH 2–6. However, some of the dissolved Sb could actually be in the form of nanoparticles instead of true dissolution. As some Sb was found from the solution, one could argue that the Tc uptake is due to dissolution and re-precipitation of Sb but the Sb_2O_3 and Sb_2O_5 reference samples (Table 2) did not show such a Tc uptake behavior. According to the MP-AES measurement, zirconium concentration in the solution was below the detection limit (0.01 mg L^{-1}) at pH 1.0–9.9 that is in agreement with the known solubility properties of ZrO_2. The low solubility of the fibers enables their use over a broad pH range without deterioration that should facilitate effective decontamination.

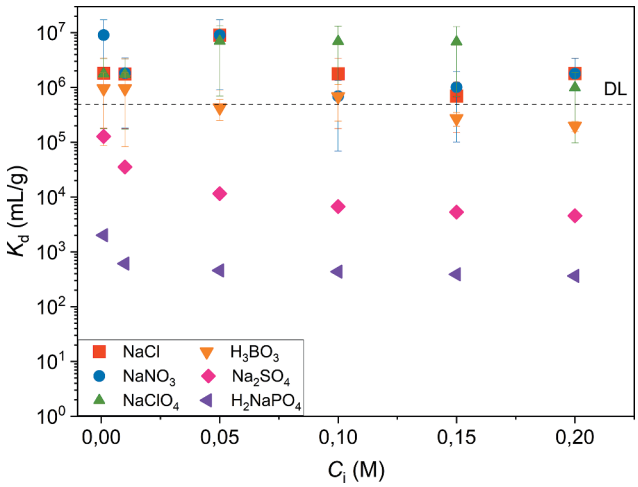

Figure 7. Effect of competing ion concentration (0.001–0.2 M) on 20 Bq mL^{-1} $^{99}TcO_4^-$ separation at pH 4.0 using 1 g L^{-1} adsorbent concentration. DL is 0.04 Bq mL^{-1}.

Table 2. TcO_4^- uptake of commercial chemical samples and fiber samples as a comparison in 0.01 M NaCl at pH 4.0.

Chemical	Uptake (%)	K_d (mL g^{-1})
m-ZrO_2	0.22 ± 1.06	2 ± 15
Sb_2O_5	15.06 ± 0.94	176 ± 18
Sb_2O_3	0.72 ± 1.05	7 ± 15
15%Sb:ZrO_2 fiber	99.98 ± 0.09	6 500 000 ± 37 600 000
10%Sb:ZrO_2 fiber	99.98 ± 0.09	6 600 000 ± 38 000 000
5%Sb:ZrO_2 fiber	99.98 ± 0.09	6 700 000 ± 38 400 000
ZrO_2 fiber	5.83 ± 0.74	61 ± 13

The effect of pH on Tc uptake. Solution pH can greatly influence the uptake of ions including TcO_4^- because pH affects both the surface charge of an adsorbent and speciation of an adsorbate. In the case of Tc(VII), TcO_4^- is the prevalent species over a wide pH range. Only below the studied pH range, Tc(VII) prevails as a neutral pertechnetic acid, $HTcO_4$, with the pK_a of 0.032, but at pH 2.0 the fraction of $HTcO_4$ is only 1.1%.[50] From the obtained results, a significant difference in TcO_4^- uptakes between the undoped ZrO_2 and Sb-doped ZrO_2 fibers can be observed, Fig. 6. At their best, the K_d values of the Sb-doped fibers were four orders of magnitude higher than the values of the ZrO_2 fibers. For the Sb-doped ZrO_2 fibers, the Sb-doping level did not seem to influence the K_d values markedly since even a low quantity of Sb(III) is sufficient to reduce a trace amount of TcO_4^-. The optimum pH range for the TcO_4^- separation was from pH 2 to 6 for all the studied fibers. The observed uptake trend is in a good agreement with a mechanism where the electrostatic attraction is holding TcO_4^- anion on the positively charged fiber surface, Equation 3. Below pH 2 a rather high fraction of neutral $HTcO_4$ is responsible for the K_d decrease as $HTcO_4$ is not electrostatically attracted by the positively charged surface whereas above pH 6 surfaces of the fibers are negative (Fig. 5) and therefore repelling the TcO_4^- anions.

$$\equiv SOH_{2+} + TcO_{4-} \leftrightarrow \equiv SOH_{2+} \ldots TcO_{4-} \quad (3)$$

The electrostatic attraction can be responsible for the TcO_4^- uptake by the undoped ZrO_2 fibers too but the mechanism cannot explain the difference in the uptake efficiencies of the undoped and Sb-doped ZrO_2 fibers. Therefore, it is concluded that the Sb doping is responsible for the uptake difference. The most probable explanation is the redox reaction between Sb and Tc as the oxidation of Sb(III) was observed in the XAS analysis (Fig. 4). In addition, the oxidation potential of Sb(III) is sufficient to reduce Tc(VII) to Tc(IV) while Sb(III) oxidizes to Sb(V). Relevant redox half reactions of Sb and Tc and their potentials are presented below, [51,52] Equations 4, 5 and 6.

$$Sb(OH)_{4-} + H2O \leftrightarrow Sb(OH)_{6-} + 2H^+ + 2e^-(E^0 = -0.363V) \quad (4)$$

$$Sb_2O_3 + 2H_2O \leftrightarrow Sb_2O_5 + 4H^+ + 4e^-(E^0 = -0.649V) \quad (5)$$

$$TcO_{4-} + 4H^+ + 3e^- \leftrightarrow TcO_2 + 2H_2O(E^0 = 0.738V) \quad (6)$$

When the half reactions of Sb_2O_3 (5) and TcO_4^- (6) are combined, the full redox reaction is obtained with the positive potential value meaning spontaneous redox reaction between Sb(III) and Tc(VII), Equation 7.

$$3Sb_2O_3 + 4TcO_{4-} + 4H^+ \leftrightarrow 3Sb_2O_5 + 4TcO_2 + 2H_2O(E^0 = 0.089V) \quad (7)$$

In the Sb-doped ZrO_2 fibers, the redox potential is probably even higher than Equation 7 indicates since Sb(III) is not prevailing as Sb_2O_3 but instead as a mixed oxide or as a surface bound species. In literature, surface bound Fe(II) has been seen as a more effective reductant than Fe(II) oxides or an aqueous Fe^{2+} and this could be possible also for Sb(III).[13,53,54] Hence, the electrostatic attraction and spontaneous reduction of TcO_4^- to Tc(IV) can together be responsible for the efficient Tc uptake. The separation efficiency decreases above pH 6 since the redox potential decreases along the rising pH and thereby lowering the uptake capability. In addition, the electrostatic repulsion between the TcO_4^- anion and the negatively charged fiber surface increases from pH 6 upwards. Therefore, the lowering redox potential and the increasing electrostatic repulsion could explain the gradually lowering K_d value along the rising pH.

However, if technetium is adsorbed after the redox reaction, the prevailing $TcO(OH)_2/TcO_2$ species should not be repelled by the negative surface.

When the TcO_4^- separation by the 10%Sb:ZrO_2 fibers was compared with ReO_4^- separation by the same fibers, a great difference was observed. In fact, the 10%Sb:ZrO_2 fibers removed ReO_4^- in a similar fashion as the undoped ZrO_2 fibers separated TcO_4^- indicating the electrostatic adsorption mechanism. Thus, ReO_4^- might not be as good surrogate for TcO_4^- separation studies as is generally thought particularly when redox reactions are plausible reasons for the uptake. The oxidation potential of Sb(III) is most probably inadequate to reduce heptavalent ReO_4^- to tetravalent ReO_2 ($E° = 0.510$ V).[51]

Reference samples

Commercial materials m-ZrO_2, Sb_2O_3 and Sb_2O_5, and the synthesized ZrO_2 and Sb-doped ZrO_2 fibers were tested for their ability to remove TcO_4^- from 0.01 M NaCl solution at pH 4, Table 2. The uptake results showed that the Sb-doped ZrO_2 fibers that contained both Zr and Sb(III) had superior performance whereas the commercial materials and the undoped ZrO_2 fibers containing only Zr or Sb(III)/Sb(V) were performing poorly by having K_d values below 200 mL g^{-1}. These observations suggest that Sb(III) is reducing Tc(VII) to Tc(IV) but zirconia surface is needed to bind Tc(IV) from the solution because Sb_2O_3 alone was not separating Tc efficiently.

Competing ions

High selectivity is essential when a trace amount of a target ion is removed from a solution containing many orders of magnitude higher concentrations of other ions or compounds. For that reason, the effects of Cl^-, NO_3^-, SO_4^{2-}, $H_2PO_4^-$, ClO_4^- and H_3BO_3 on the TcO_4^- uptake were examined, Fig. 7. The results show that the presence of Cl^- and NO_3^- did not weaken the TcO_4^- uptake in the investigated concentration range. Instead, Gao *et al.*[14] observed increasing NO_3^- concentration to decrease ReO_4^- adsorption capacity of ZrO_2 @rGO significantly but the result could be related to a much higher concentration of perrhenate than used here for the radioactive pertechnetate or to competing adsorption to the same adsorption sites. Despite their similar stereo structure, the TcO_4^- remediation remained unaffected by ClO_4^- in our experiments since Sb(III) was unable to reduce ClO_4^- and 10%Sb:ZrO_2 showed no affinity for ClO_4^- adsorption. In contrast, it has been reported that remediation of TcO_4^- by activated carbon was significantly reduced in the presence of ClO_4^- as the ions have similar tetrahedral structure and probably high affinity to the same adsorption sites.[15] Additionally, our experiment showed that H_3BO_3 decreased the K_d value of TcO_4^- only slightly. This is an extremely important result since H_3BO_3 is used in nuclear industry as a neutron absorber to regulate the power of reactors. Therefore, TcO_4^- waste solutions can contain significant concentrations of H_3BO_3 without disturbing the TcO_4^- uptake. Instead, SO_4^{2-} and $H_2PO_4^-$ decreased the K_d value of TcO_4^- significantly even at the lowest 0.001 M concentration but above 0.05 M further addition of either anion did not significantly lower the K_d values. Most probably, the negative effects of sulfate and phosphate anions on the uptake of other anions derive from their strong interaction with zirconia surface. When zirconia adsorbs negatively charged sulfate and phosphate ions, its surface charge changes to negative and the electrostatic attraction changes to a repulsion between the surface and other anions, Fig. A6. It is also possible that Tc forms complexes with sulfate and phosphate anions that could somewhat influence the TcO_4^- uptake. However, concentrations of sulfate and phosphate anions in nuclear wastewaters are low and therefore their influence can be considered low in real applications. From the studied compounds, only NO_3^- and ClO_4^- would have sufficient oxidation potential for the Sb(III) oxidation but the slow kinetics of NO_3^- and ClO_4^- reduction are diminishing their influence on the TcO_4^- removal process.[55]

Kinetics

Fast uptake kinetics is necessary particularly when large volumes of water are to be treated. For that reason, the TcO_4^- uptake kinetics of the Sb-doped ZrO_2 fibers was demonstrated in a batch experiment where ground fiber powder was mixed with TcO_4^- containing solution with a magnetic stirrer, Fig. 8. The TcO_4^- uptake was fast for all the studied fibers. At the first time point, the K_d values of Tc exceeded 1 000 mL g^{-1}, which are in percentages more precisely 67%, 80%, and 86% for 5%Sb:ZrO_2, 10%Sb:ZrO_2, and 15%Sb:ZrO_2, respectively. Thus, it seems that in the beginning of the experiment the highest separation was achieved with the fibers that have the highest Sb concentration. However, after a few minutes the order of the K_d values turns into the opposite. The fibers containing 5%Sb:ZrO_2 reach the detection limit first, in 20 minutes, the 10 mol% Sb fibers in 30 minutes, and the 15 mol% Sb fibers in 60 minutes. Thus, the kinetics does not seem to correlate with the maximum adsorption capacity observed in the column experiments (Fig. 9). Even though Sb(III) is needed for the TcO_4^- reduction, Sb can also have an inhibitory effect on the TcO_4^- uptake that slows down the reaction. As seen in the zeta potential experiment (Fig. 5), the

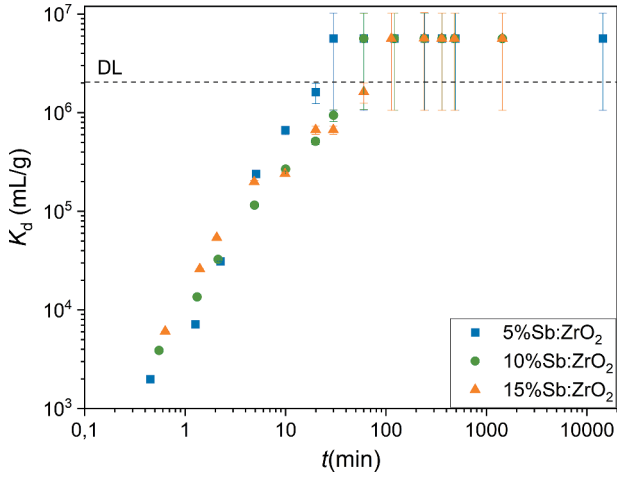

Figure 8. Distribution coefficient of 20 Bq mL^{-1} TcO_4^- as a function of time in 0.01 M NaCl at pH 4.0 using 1 g L^{-1} adsorbent concentration. DL is 0.02 Bq mL^{-1}.

surface charge decreased when the Sb-doping level increased weakening the electrostatic attraction between TcO_4^- and the fiber surface that could explain the observed behavior. Furthermore, increasing the Sb-doping level leads to a higher Sb concentration on the fiber surface offering less zirconia adsorption sites for the reduced Tc that can also have a retarding influence on the Tc uptake.

Column separation

Packed bed columns are one of the easiest approaches to remove radionuclides from water solutions. Contaminated water is simply fed through a column and clean solution after the bed can be discharged after proper monitoring. For that reason, such an experiment was conducted for the Sb-doped ZrO_2 fibers in a smaller scale, Fig. 9a. In this laboratory experiment, the TcO_4^- solution was fed through a 1 cm diameter column and the breakthrough of TcO_4^- after 5%Sb:ZrO_2, 10%Sb:ZrO_2 and 15%Sb:ZrO_2 beds was followed to examine the behavior of the materials in dynamic use. The observed performance was excellent before the breakthrough because the TcO_4^- concentration stayed below the detection limit. TcO_4^- breakthrough began first with the 5%Sb:ZrO_2 fibers but surprisingly the next breakthrough was observed for the 15%Sb:ZrO_2 fiber column instead of the 10%Sb:ZrO_2 column, which was the last one to be exhausted. This was also the order of the TcO_4^- uptake capacities that were 2.1 ± 0.1, 3.6 ± 0.1 and 3.5 ± 0.1 μmol/g for 5%Sb:ZrO_2, 10%Sb:ZrO_2 and 15%Sb:ZrO_2 fibers, respectively. Hence, the uptake capacities are not fully following the amount of the Sb concentration in the fibers. The most probable reason for the inconsistency is a higher portion of oxidized Sb(V) in the calcined 15%Sb:ZrO_2 fibers. However, an accurate calculation of the Sb(III)/Sb(V) ratio and hence the amount of Sb(III) in the fiber structure would require a synchrotron XAS measurement. Despite the rather limited quality of our XAS data, the major changes in the oxidation states of Sb can be qualitatively observed. The XAS spectrum of the Tc loaded 10%Sb:ZrO_2 fibers showed (Fig. 4.) that after the Tc loading Sb(III) was almost fully oxidized to Sb(V). The result indicates that the 100% TcO_4^- breakthrough was reached when the reactive Sb(III) was consumed as a consequence of the reduction of Tc(VII) and dissolved O_2.

Steepness of the breakthrough slopes follows the order 5%Sb:ZrO_2, 10%Sb:ZrO_2 and 15%Sb:ZrO_2 that is the same order as observed in the kinetic experiment. As the contact time between the solution and the fibers is equal for all columns, the kinetics together with the capacity dictate how large fraction of Tc is removed. When the column approaches full exhaustion, in other words, when the reaction zone in the column reaches the bottom, breakthrough begins. After this point, the contact time between TcO_4^- and active sites is gradually shortened that causes an increasing fraction of TcO_4^- to pass through the column. Therefore, a material with the fastest kinetics results in the steepest rise of the

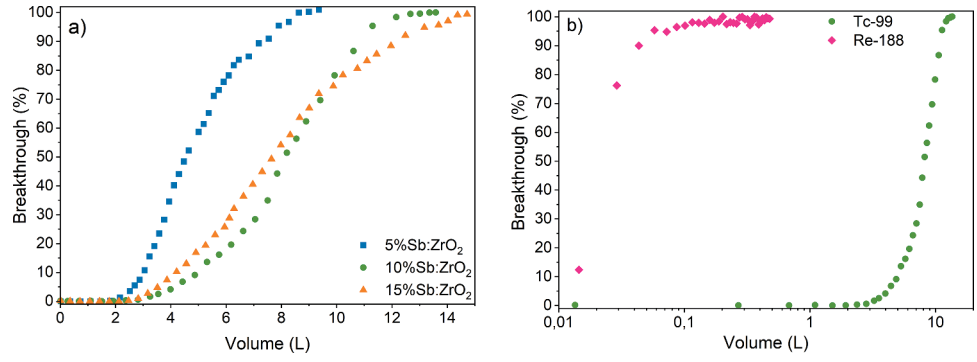

Figure 9. Breakthrough of the columns a) packed with 0.25 g Sb-doped ZrO_2 fibers for solution with 10 kBq L^{-1} ^{99}Tc in 0.01 M NaCl at pH 4.0. b) Breakthrough of the column packed with 0.25 g of 10%Sb:ZrO_2 fiber for 10 kBq L^{-1} ^{99}Tc and 54.2 kBq L^{-1} ^{188}Re in 0.01 M NaCl at pH 4.0 on a logarithmic scale.

breakthrough since the column having the shortest reaction zone is the closest to full exhaustion before the breakthrough begins. Due to the lower Sb-doping level of 5%Sb:ZrO_2, a larger fraction of Zr is exposed on the surface compared to 10%Sb:ZrO_2 and 15%Sb:ZrO_2, which together with the highest zeta potential enables fast remediation of TcO_4^-. From the studied fibers, 10%Sb:ZrO_2 is seen as the most prominent for TcO_4^- removal. The 10%Sb:ZrO_2 fibers have the largest Tc uptake capacity and higher degree of utilization (V_{BT}/V_{TOT}) that enable their longer lasting use compared to 5%Sb:ZrO_2 and 15%Sb:ZrO_2. The situation could change if the Sb in the 15%Sb:ZrO_2 fibers would be fully reduced to Sb(III). In addition, the operation of the column in anaerobic conditions could considerably improve the performance of all columns as then the dissolved O_2 would not participate in the oxidation of Sb(III).

The uptake of TcO_4^- and ReO_4^- by 10%Sb:ZrO_2 was further compared with the column experiment. A similar 10%Sb:ZrO_2 column test as done for TcO_4^- was conducted for $^{188}ReO_4^-$, Fig. 9b. The difference in the breakthrough is drastic as $^{188}ReO_4^-$ reaches 10% breakthrough immediately in the first fraction, after 0.015 L, while the same takes approximately 5.0 L for $^{99}TcO_4^-$ meaning over 300-fold difference even though the TcO_4^- concentration ($1.11 \cdot 10^{-7}$ M) in the feed solution is several orders of magnitude higher than the ReO_4^- concentration ($5.51 \cdot 10^{-15}$ M). This result confirms the observation from the pH experiment that ReO_4^- cannot be used as a TcO_4^- surrogate with reductive materials before proper initial testing.

Conclusions

In this study, electroblown ZrO_2 and Sb-doped ZrO_2 submicron fibers with 5, 10 and 15 cation% of Sb were synthesized for TcO_4^- separation. All the fibers had mainly the tetragonal ZrO_2 structure but some monoclinic ZrO_2, which is the inactive form of zirconia, was observed in the ZrO_2 and 15%Sb:ZrO_2 fibers. The fibers had high length-to-diameter ratio, smooth surfaces and high specific surface areas, 43–59 $m^2\ g^{-1}$. The Sb-doping levels were close to the designed values but a certain loss of Sb during the synthesis was observed. Sb was added into the synthesis solution as Sb(III) but partial oxidation of Sb(III) occurred most probably during the calcination process.

The fiber synthesis was designed to produce fibers with great TcO_4^- uptake properties that were studied with batch and dynamic column experiments. The hypothesis was that Sb(III) in the Sb-doped ZrO_2 fibers would reduce Tc(VII) to Tc(IV) that would be retained by the zirconia surface. Indeed, the oxidation of Sb(III) to Sb(V) during the column operation was observed which indicates that Sb(III) was oxidized by TcO_4^- and dissolved O_2 in the solution. From all the studied fibers, the 10%Sb:ZrO_2 fibers had the highest capacity and the best performance because of their seemingly high Sb(III)/Sb(V) ratio. The influence of Sb(III) on the Tc uptake capability of the fibers was the most evident when the performance of the Sb-doped ZrO_2 fibers was compared with the undoped ZrO_2 revealing several orders of magnitude higher K_d values for the doped fibers. The optimal pH for the separation was below the pH_{PZC} because of the electrostatic attraction between TcO_4^- and the positively charged surface but the separation remained on a high level throughout the studied range from pH 1 to 10. The Tc uptake kinetics was fast and the separation was unaffected by Cl^-, NO_3^- and ClO_4^- ions in the solution and H_3BO_3 decreased K_d values only slightly which is very important in the decontamination of nuclear waste solutions. In addition, as the reduction chemistry of Re differs significantly from Tc, the Re separation was much less efficient. Therefore, care must be taken when Re is used as a Tc surrogate particularly when the uptake material has reductive properties. Based on the conducted experiments, the Sb-doped ZrO_2 fibers are seen highly prominent materials for TcO_4^- sequestration even in aerobic conditions due to their selectivity, fast kinetics and suitability for the final disposal in the ceramic form. Future research should be targeted to synchrotron quality XAS measurements on Sb and Tc in the fibers, the full reduction of Sb to Sb(III) before adsorption experiments and uptake studies in anaerobic conditions.

Acknowledgements

Authors would like to acknowledge the financial support of Fortum Power and Heat Oy and Doctoral School of Natural Sciences (University of Helsinki). We would also like to thank Ilkka Välimaa for conducting the XRF measurement and Kaisu Ainassaari for BET analysis.

Funding

This work was supported by the Doctoral school in natural sciences; Fortum Power and Heat Oy.

ORCID

Satu Lönnrot http://orcid.org/0000-0003-1114-8599
Valtteri Suorsa http://orcid.org/0000-0003-1544-5283

Conflicts of interests

No potential conflict of interest was reported by the authors.

References

[1] IAEA. Live Chart of Nuclides - Nuclear structure and decay data, 2020 (January 31), 2019.

[2] Anders, E. The Radiochemistry of Technetium. *Nuclear Science Series*., NAS-NS 3021, 1960.

[3] Liu, D. J.; Yao, J.; Wang, B.; Bruggeman, C.; Maes, N. Solubility Study of Tc(IV) in a Granitic Water. *Radiochim. Acta.* 2007, 95(9), 523.

[4] Xiao, C.; Khayambashi, A.; Wang, S. Separation and Remediation of $^{99}TcO_4^-$ From Aqueous Solutions. *Chem. Mater.* 2019, 31(11), 3863.

[5] Li, J.; Dai, X.; Zhu, L.; Xu, C.; Zhang, D.; Silver, M. A.; Li, P.; Chen, L.; Li, Y.; Zuo, D.; et al. $^{99}TcO_4^-$ Remediation by a Cationic Polymeric Network. *Nat. Commun.* 2018, 9(1), 3007.

[6] Liang, L.; Gu, B.; Yin, X. Removal of Technetium-99 from Contaminated Groundwater with Sorbents and Reductive Materials. *Separ. Technol.* 1996, 6(2), 111.

[7] Chakravarty, R.; Bahadur, J.; Lohar, S.; Sarma, H. D.; Sen, D.; Mishra, R.; Chakraborty, S.; Dash, A. Solid State Synthesis of Mesoporous Alumina: A Viable Strategy for Preparation of an Advanced Nanosorbent for $^{99}Mo/^{99m}Tc$ Generator Technology. *Micropor. Mesopor. Mat.* 2019, 287, 271.

[8] Drout, R. J.; Otake, K.; Howarth, A. J.; Islamoglu, T.; Zhu, L.; Xiao, C.; Wang, S.; Farha, O. K. Efficient Capture of Perrhenate and Pertechnetate by a Mesoporous Zr Metal-Organic Framework and Examination of Anion Binding Motifs. *Chem. Mater.* 2018, 30(4), 1277.

[9] Sheng, D.; Zhu, L.; Dai, X.; Xu, C.; Li, P.; Pearce, I. C.; Xiao, C.; Chen, J.; Zhou, R.; Duan, T.; et al. Successful Decontamination of (Tco_4^-)-tc-99 in Groundwater at Legacy Nuclear Sites by a Cationic Metal-Organic Framework with Hydrophobic Pockets. *Angew. Chem. Int. Edit.* 2019, 58(15), 4968.

[10] Zhu, L.; Sheng, D.; Xu, C.; Dai, X.; Silver, M. A.; Li, J.; Li, P.; Wang, Y.; Wang, Y.; Chen, L.; et al. Identifying the Recognition Site for Selective Trapping of $^{99}TcO_4^-$ In a Hydrolytically Stable and Radiation Resistant Cationic Metal–Organic Framework. *J. Am. Chem. Soc.* 2017, 139(42), 14873.

[11] Sheng, D.; Zhu, L.; Xu, C.; Xiao, C.; Wang, Y.; Wang, Y.; Chen, L.; Diwu, J.; Chen, J.; Chai, Z.; et al. Efficient and Selective Uptake of TcO_4^- By a Cationic Metal–Organic Framework Material with Open Ag^+ Sites. *Environ. Sci. Technol.* 2017, 51(6), 3471.

[12] Liu, D.; Fan, X. Adsorption Behavior of Tc-99 on Fe, Fe_2O_3 and Fe_3O_4. *J. Radioanal. Nucl. Ch.* 2005, 264(3), 691.

[13] Boglaienko, D.; Emerson, H. P.; Katsenovich, Y. P.; Levitskaia, T. G. Comparative Analysis of ZVI Materials for Reductive Separation of Tc-99(VII) from Aqueous Waste Streams. *J. Hazard. Mater.* 2019, 380 (120836).

[14] Gao, Y.; Chen, K.; Tan, X.; Wang, X.; Alsaedi, A.; Hayat, T.; Chen, C. Interaction Mechanism of Re(VII) with Zirconium Dioxide Nanoparticles Archored onto Reduced Graphene Oxides. *ACS Sustain. Chem. Eng.* 2017, 5(3), 2163.

[15] Galambos, M.; Dano, M.; Viglasova, E.; Krivosudsky, L.; Rosskopfova, O.; Novak, I.; Berek, D.; Rajec, P. Effect of Competing Anions on Pertechnetate Adsorption by Activated Carbon. *J. Radioanal. Nucl. Ch.* 2015, 304 (3), 1219.

[16] Viglasova, E.; Dano, M.; Galambos, M.; Rosskopfova, O.; Rajec, P.; Novak, I. Column Studies for the Separation of Tc-99m Using Activated Carbon. *J. Radioanal. Nucl. Ch.* 2016, 307(1), 591.

[17] Gu, B.; Dowlen, K. E.; Liang, L.; Clausen, J. L. Efficient Separation and Recovery of Technetium-99 from Contaminated Groundwater. *Separ. Technol.* 1996, 6 (2), 123.

[18] Li, D.; Seaman, J. C.; Murph, S. E. H.; Kaplan, I. D.; Taylor-Pashowa, K.; Feng, R.; Chang, H.; Tandukar, M. Porous Iron Material for TcO_4^- and ReO_4^- Sequestration from Groundwater under Ambient Oxic Conditions. *J. Hazard. Mater.* 2019, 374, 177.

[19] Calderon, B.; Fullana, A. Heavy Metal Release Due to Aging Effect during Zero Valent Iron Nanoparticles Remediation. *Water Res.* 2015, 83, 1.

[20] Guan, X.; Sun, Y.; Qin, H.; Li, J.; Lo, I. M. C.; He, D.; Dong, H. The Limitations of Applying Zero-valent Iron Technology in Contaminants Sequestration and the Corresponding Countermeasures: The Development in Zero-valent Iron Technology in the Last Two Decades (1994-2014). *Water Res.* 2015, 75, 224.

[21] Koivula, R.; Harjula, R. Selective Sorption of Technetium on Antimony-Doped Tin Dioxide. *Sep. Sci. Technol.* 2011, 46(2), 315.

[22] Holopainen, J.; Ritala, M. Rapid Production of Bioactive Hydroxyapatite Fibers via Electroblowing. *J. Eur. Ceram. Soc.* 2016, 36(13), 3219.

[23] Holopainen, J.; Heikkila, M. J.; Salmi, L. D.; Ainassaari, K.; Ritala, M. Zeolitic Imidazole Framework-8 (ZIF-8) Fibers by Gas-phase Conversion of Electroblown Zinc Oxide and Aluminum Doped Zinc Oxide Fibers. *Micropor. Mesopor. Mat.* 2018, 267, 212.

[24] Kong, C. S.; Yoo, W. S.; Lee, K. Y.; Kim, H. S. Nanofiber Deposition by Electroblowing of PVA (Polyvinyl Alcohol). *J. Mater. Chem.* 2009, 44(4), 1107.

[25] Pokorny, M.; Rassushin, V.; Wolfova, L.; Velebny, V. Increased Production of Nanofibrous Materials by Electroblowing from Blends of Hyaluronic Acid and Polyethylene Oxide. *Polym. Eng. Sci.* 2016, 56(8), 932.

[26] Lönnrot, S.; Suorsa, V.; Paajanen, J.; Hatanpää, T.; Ritala, M.; Koivula, R. Submicron Fibers as a Morphological Improvement of Amorphous Zirconium Oxide Particles and Their Utilization in Antimonate (Sb(v)) Removal. *RSC Adv.* 2019, 9(39), 22355.

[27] Paajanen, J.; Lönnrot, S.; Heikkilä, M.; Meinander, K.; Kemell, M.; Hatanpää, T.; Ainassaari, K.; Ritala, M.; Koivula, R. Novel Electroblowing Synthesis of Submicron Zirconium Dioxide Fibers: Effect of Fiber Structure on Antimony(v) Adsorption. *Nanoscale Adv.* 2019, 1(11), 4373.

[28] Basahel, S. N.; Ali, T. T.; Mokhtar, M.; Narasimharao, K. Influence of Crystal Structure of Nanosized ZrO_2 on

Photocatalytic Degradation of Methyl Orange. *Nanoscale. Res. Lett.* 2015, 10(73).
[29] Deshmane, V. G.; Adewuyi, Y. G. Synthesis of Thermally Stable, High Surface Area, Nanocrystalline Mesoporous Tetragonal Zirconium Dioxide (Zro_2): Effects of Different Process Parameters. *Micropor. Mesopor. Mat.* 2012, 148(1), 88.
[30] Abu El-Fadl, A.; Eltokhey, A. M.; Abu-Sehley, A. A.; El-Attar, H. M. Fabrication and Analysis of the Structural Phase Transition of ZrO_2 Nanoparticles Using Modified Facile Sol-gel Route. *Phase. Transit.* 2019, 92(1), 36.
[31] Zink, N.; Emmerling, F.; Haeger, T.; Panthoefer, M.; Tahir, M. N.; Kolb, U.; Tremel, W. Low Temperature Synthesis of Monodisperse Nanoscaled ZrO_2 with a Large Specific Surface Area. *Dalton. T.* 2013, 42(2), 432.
[32] Qin, H.; Guo, W.; Huang, X.; Gao, P.; Xiao, H. Preparation of Yttria-stabilized ZrO_2 Nanofiltration Membrane by Reverse Micelles-mediated Sol-gel Process and Its Application in Pesticide Wastewater Treatment. *J. Eur. Ceram. Soc.* 2020, 40(1), 145.
[33] Wang, S.; Xia, G. A Facile Low-cost Preparation of High-k ZrO2 Dielectric Films for Superior Thin-film Transistors. *Ceram. Int.* 2019, 45(17, B), 23666.
[34] Wang, H.; Lin, S.; Yang, S.; Yang, X.; Song, J.; Wang, D.; Wang, H.; Liu, Z.; Li, B.; Fang, M.; et al. High-Temperature Particulate Matter Filtration with Resilient Yttria-Stabilized ZrO_2 Nanofiber Sponge. *Small.* 2018, 14, 19.
[35] Rigney, M.; Funkenbusch, E.; Carr, P. Physical and Chemical Characterization of Microporous Zirconia. *J. Chromatogr.* 1990, 499, 291.
[36] Su, Y.; Yang, W.; Sun, W.; Li, Q.; Shang, J. K. Synthesis of Mesoporous Cerium-zirconium Binary Oxide Nanoadsorbents by a Solvothermal Process and Their Effective Adsorption of Phosphate from Water. *Chem. Eng. J.* 2015, 268, 270.
[37] Cui, H.; Li, Q.; Gao, S.; Shang, J. K. Strong Adsorption of Arsenic Species by Amorphous Zirconium Oxide Nanoparticles. *J. Ind. Eng. Chem.* 2012, 18(4), 1418.
[38] Honkanen, A.; Ollikkala, S.; Ahopelto, T.; Kallio, A.; Blomberg, M.; Huotari, S. Johann-type Laboratory-scale X-ray Absorption Spectrometer with Versatile Detection Modes. *Rev. Sci. Instrum.* 2019, 90(3), 033107.
[39] Peniche, C.; Zaldivar, D.; Pazos, M.; Paz, S.; Bulay, A.; Roman, J. Study of the Thermal-degradation of poly (N-vinyl-2-pyrrolidone) by thermogravimetry-FTIR. *J. Appl. Polym. Sci.* 1993, 50(3), 485.
[40] Smirnov, A.; Solis Pinargote, N. W.; Peretyagin, N.; Pristinskiy, Y.; Peretyagin, P.; Bartolome, J. F. Zirconia Reduced Graphene Oxide Nano-Hybrid Structure Fabricated by the Hydrothermal Reaction Method. *Materials*. 2020, 13(3), 687.
[41] Rao, T. N.; Hussain, I.; Lee, J. E.; Kumar, A.; Koo, B. H. Enhanced Thermal Properties of Zirconia Nanoparticles and Chitosan-Based Intumescent Flame Retardant Coatings. *Appl. Sci. -Basel.* 2019, 9(17), 3464.
[42] Shannon, R.;. Revised Effective Ionic-radii and Systematic Studies of Interatomic Distances in Halides and Chalcogenides. *Acta Crystallogr. A.* 1976, 32, 751.
[43] Cavaliere, S.; Jimenez-Morales, I.; Ercolano, G.; Savych, I.; Jones, D.; Roziere, J. Highly Stable PEMFC Electrodes Based on Electrospun Antimony-Doped SnO_2. *Chemelectrochem.* 2015, 2(12), 1966.
[44] Zhang, D.; Deng, Z.; Zhang, J.; Chen, L. Microstructure and Electrical Properties of Antimony-doped Tin Oxide Thin Film Deposited by Sol-gel Process. *Mat. Chem. Phys.* 2006, 98(2–3), 353.
[45] Rodriguez-Albelo, L. M.; Lopez-Maya, E.; Hamad, S.; Ruiz-Salvador, A.; Calero, S.; Navarro, J. A. R. Selective Sulfur Dioxide Adsorption on Crystal Defect Sites on an Isoreticular Metal Organic Framework Series. *Nat. Commun.* 2017, 8, 14457.
[46] Gulino, A.; Egdell, R.; Fragala, I. Low-temperature Stabilisation of Tetragonal Zirconia by Antimony. *J. Mater. Chem.* 1996, 6(11), 1805.
[47] Gulino, A.; Egdell, R.; Baratta, G.; Compagnini, G.; Fragala, I. Surface Segregation and Effect of Mechanical Stress on Sb-stabilised Tetragonal Zirconia. *J. Mater. Chem.* 1997, 7(6), 1023.
[48] Wang, L. Y.; Lee, M. S. A Review on the Aqueous Chemistry of Zr(IV) and Hf(IV) and Their Separation by Solvent Extraction. *J. Ind. Eng. Chem.* 2016, 39, 1.
[49] Leuz, A.; Johnson, C. A. Oxidation of Sb(III) to Sb(V) by O_2 and H_2O_2 in Aqueous Solutions. *Geochim. Cosmochim. Acta.* 2005, 69(5), 1165.
[50] Nakashima, T.; Lieser, K. H. Proton Association of Pertechnetate, Perrhenate and Perchlorate Anions. *Radiochim. Acta.* 1985, 38(4), 203.
[51] Rumble, J. R.; Lide, D. R.; Bruno, T. J. *CRC Handbook of Chemistry and Physics*, 98th ed.; Internet version 2018; CRC Press, Taylor and Francis Group: Boca Raton, 2017.
[52] Bard, A. J.; Parsons, R.; Jordan, J. *Standard Potentials in Aqueous Solution*; Dekker: New York, 1985.
[53] Zachara, J. M.; Heald, S. M.; Jeon, B.; Kukkadapu, R. K.; Liu, C.; McKinley, J. P.; Dohnalkova, A. C.; Moore, D. A. Reduction of Pertechnetate [Tc(vii)] by Aqueous Fe(II) and the Nature of Solid Phase Redox Products. *Geochim. Cosmochim. Acta.* 2007, 71(9), 2137.
[54] Bae, S.; Hanna, K. Reactivity of Nanoscale Zero-Valent Iron in Unbuffered Systems: Effect of pH and Fe(II) Dissolution. *Environ. Sci. Technol.* 2015, 49(17), 10536.
[55] Weller, M.; Overton, T.; Rourke, J.; Armstrong, F. *Inorganic Chemistry*, Sixth ed.; Oxford University Press: Oxford, 2014.